Engineering 6 (2020) 1276–1284

Contents lists available at ScienceDirect

Engineering

journal homepage: www.elsevier.com/locate/eng

Research
Medical Additive Manufacturing—Article

3D Printing of Cell-Container-Like Scaffolds for Multicell Tissue Engineering

Xiaoya Wang [a,b,#], Meng Zhang [a,b,#], Jingge Ma [a,b], Mengchi Xu [a,b], Jiang Chang [a,b], Michael Gelinsky [c], Chengtie Wu [a,b,*]

[a] State Key Laboratory of High Performance Ceramics and Superfine Microstructure, Shanghai Institute of Ceramics, Chinese Academy of Sciences, Shanghai 200050, China
[b] Center of Materials Science and Optoelectronics Engineering, University of Chinese Academy of Sciences, Beijing 100049, China
[c] Center for Translational Bone, Joint and Soft Tissue Research, University Hospital Carl Gustav Carus & Faculty of Medicine, Technische Universität Dresden, Dresden 01307, Germany

ARTICLE INFO

Article history:
Received 2 July 2019
Revised 6 December 2019
Accepted 10 May 2020
Available online 6 August 2020

Keywords:
3D cell containers
Non-contact multicellular coculture
Interactions
Angiogenesis
Osteogenesis

ABSTRACT

The development of an engineered non-contact multicellular coculture model that can mimic the *in vivo* cell microenvironment of human tissues remains challenging. In this study, we successfully fabricated a cell-container-like scaffold composed of β-tricalcium phosphate/hydroxyapatite (β-TCP/HA) bioceramic that contains four different pore structures, including triangles, squares, parallelograms, and rectangles, by means of three-dimensional (3D) printing technology. These scaffolds can be used to simultaneously culture four types of cells in a non-contact way. An engineered 3D coculture model composed of human bone-marrow-derived mesenchymal stem cells (HBMSCs), human umbilical vein endothelial cells (HUVECs), human umbilical vein smooth muscle cells (HUVSMCs), and human dermal fibroblasts (HDFs) with a spatially controlled distribution was constructed to investigate the individual or synergistic effects of these cells in osteogenesis and angiogenesis. The results showed that three or four kinds of cells cocultured in 3D cell containers exhibited a higher cell proliferation rate in comparison with that of a single cell type. Detailed studies into the cell–cell interactions between HBMSCs and HUVECs revealed that the 3D cell containers with four separate spatial structures enhanced the angiogenesis and osteogenesis of cells by amplifying the paracrine effect of the cocultured cells. Furthermore, the establishment of multicellular non-contact systems including three types of cells and four types of cells, respectively, cocultured in 3D cell containers demonstrated obvious advantages in enhancing osteogenic and angiogenic differentiation in comparison with monoculture modes and two-cell coculture modes. This study offers a new direction for developing a scaffold-based multicellular non-contact coculture system for tissue regeneration.

1. Introduction

The ultimate goal of tissue engineering is to obtain a tissue or organ that is native-like at the structural and functional levels [1–3]. Thus far, however, tissue engineering technology is still facing challenges in mimicking the complex structure and function of biological tissues [4,5]. Human body tissues contain more than 200 cell types, and most of these tissues are composed of a variety of cells, which are required to maintain normal tissue function. For this reason, it is currently impossible to construct complex three-dimensional (3D) tissues and organs *in vitro* [6]. Therefore, developing *in vitro* cell culture models that are similar to *in vivo* cell niches in order to investigate cell proliferation, differentiation, and cell–cell interactions is essential for the fabrication of engineered tissues. *In vitro* models of cell behavior play a key role in mimicking native tissues and organs. Conventional two-dimensional (2D) cell culture models such as cell culture plates cannot provide the proper microenvironment for cells to maintain natural morphologies or efficient communications [7,8]. Cells cultured on 2D surfaces are thought to show improved cell proliferation but inhibited cell differentiation [9]. In addition, natural tissues are complex systems consisting of two or more types of cells that communicate with one another through vital movement [10]. Although establishing a coculture system on a cell

* Corresponding author.
E-mail address: chengtiewu@mail.sic.ac.cn (C. Wu).
# These authors contributed equally to this work.

https://doi.org/10.1016/j.eng.2020.08.001

culture plate can enhance cell–cell interaction and communication, the cocultured cells on 2D surfaces cannot be organized spatially as in an *in vivo* environment [7,11,12]. Thus, a more appropriately engineered model is needed to create growth conditions and solve problems.

Previously, 3D cell culture models have been developed to offer relatively natural morphologies and cellular functions in the form of scaffold-free or scaffold-based culture systems, depending on tissue structures and functions. Bone tissue is known to be a complex system that contains many types of cells ordered in the extracellular matrix in response to mechanical and physiological stimuli [13]. Scaffold-based culture systems are advantageous in that they provide mechanical support and tissue continuity. Therefore, scaffold-based coculture systems have been established for research on cell–cell interactions and individual or synergistic effects in bone tissue regeneration. For example, the coculture of human bone-marrow-derived mesenchymal stem cells (HBMSCs) and human umbilical vein endothelial cells (HUVECs) on β-tricalcium phosphate (β-TCP) scaffolds exhibits greater alkaline phosphatase (ALP) activity than an HBMSC monoculture [14]. However, most scaffold-based coculture systems mix different types of cells together, making it impossible to distinguish the specific contributions of direct intercellular contact and the paracrine effect, respectively [15]. In addition, the various cells in human tissues usually exhibit a certain non-contact spatial arrangement, so simply mixing cells together does not accurately simulate their *in vivo* state [7]. For indirect coculture systems, electrospun scaffolds [16] and multilayered hydrogels [17] have been used by means of different types of splicing. However, to the best of our knowledge, non-contact coculture models comprising three or four different kinds of cells have not yet been established. It is difficult to establish a non-contact multicellular coculture system in an integrated scaffold that can permit cells to interact with their surroundings in a 3D environment.

3D printing technology provides a valuable pathway for implementing the fabrication of complex structural scaffolds that can serve as cell carriers to realize precise cell seeding [18]. In this study, we fabricated a β-TCP/hydroxyapatite (HA) biphasic bioceramic cell container with four different pore structures including triangles, squares, parallelograms, and rectangles integrated together by means of 3D printing technology. Bone-related cells including HBMSCs, HUVECs, human umbilical vein smooth muscle cells (HUVSMCs), and human dermal fibroblasts (HDFs) were inoculated in the different pores of the cell containers to investigate their individual or synergistic effects in osteogenesis and angiogenesis. Four kinds of cells inoculated in a 2D cell culture plate were simultaneously set as the control.

To the best of our knowledge, this is the first report of a four-cell non-contact coculture system within a single integrated cell container that mimics the cell niches in bone tissue. This work provides a research model for studying the mechanism of multicellular interactions and indicates a direction for developing a scaffold-based multicellular coculture system with the ultimate goal of tissue regeneration.

2. Materials and methods

2.1. Materials

β-TCP/HA powders were purchased from Kunshan Chinese Technology New Materials Co., Ltd. (China) and filtered through a 200 mesh sieve. Pluronic F-127 (Sigma-Aldrich, USA) was dissolved to form 20 wt% aqueous solution as the binder. A homogenous printable ink was then prepared by mixing 4 g β-TCP/HA with 2 g Pluronic F-127 solution.

2.2. Design and fabrication of 3D cell containers

An integral framework divided into four parts with different pore structures including triangles, squares, parallelograms, and rectangles was designed using computer-aided design (CAD). To ensure that the cell containers could hold the four different cell types independently within the corresponding parts, all of the walls, bottom, and boundaries among different microstructure parts were seamlessly connected. The dimensions of the cell containers for studying cell proliferation were 12 mm × 12 mm × 4.8 mm, while a 24 mm × 24 mm × 4 mm geometrically similar cell container was designed for the cell differentiation experiments. The cell container was then fabricated using an extrusion-based BioScaffolder (GeSiM, Germany). To make the extrusion wire rod consistent and coherent, the moving speed of the print head was set at 4–6 $mm \cdot s^{-1}$ and the extrusion pressure was set at 2–4 bar (1 bar = 10^5 Pa) at room temperature. After the printing process, the green bodies were dried at room temperature for 24 h and then sintered at 1100 °C for 3 h with a heating rate of 2 $°C \cdot min^{-1}$ to acquire pure ceramic cell containers.

2.3. Characterization of 3D cell containers

The phase compositions of the β-TCP/HA cell containers were measured by X-ray diffraction (XRD; D8 ADVANCE, Bruker, Germany). The three orthographic views of the cell containers were observed by digital camera (Nikon, Japan), while the four kinds of microstructure were characterized by optical microscopy (S6D, Leica, Germany).

2.4. Cell culture and the establishment of a multicellular coculture system

HBMSC and HBMSC culture mediums were purchased from Cyagen Biosciences Inc. (China). HUVECs were isolated according to the method described previously [19] and cultured in endothelial cell medium (Sciencell, USA). HUVSMCs and smooth muscle cell medium were purchased from STEMCELL technologies Inc. (Canada). HDFs were obtained in accordance with previous methods [20] and grown in Dulbecco's modification of Eagle's medium (DMEM) (high glucose, with the addition of 10% fetal bovine serum and 1% penicillin–streptomycin). The cell-seeding density was 50 000 cells per scaffold for the cell proliferation experiment and 800 000 cells per scaffold for the quantitative real-time polymerase chain reaction (qRT-PCR) experiment, which are constants for either monoculture or coculture. For two-cell coculture, HBMSCs were seeded on the rectangular and square parts, while HUVECs were seeded on the triangular and parallelogram parts of the scaffold. The seeding ratio of HBMSCs and HUVECs was 1:1. For three-cell coculture, HBMSCs were seeded on the rectangular and square parts while HUVECs and HUVSMCs were seeded on the parallelogram and triangular parts of the scaffold, respectively. The seeding ratio of HBMSCs, HUVECs, and HUVSMCs was 2:1:1. For four-cell coculture, HBMSCs, HUVECs, HUVSMCs, and HDFs were seeded on the square, parallelogram, triangular, and rectangular parts of the scaffold, respectively. The seeding ratio of HBMSCs, HUVECs, HUVSMCs, and HDFs was 1:1:1:1. For the 2D culture model, the cells were monocultured or cocultured on cell culture plates with the same cell-seeding densities and ratios as in the 3D culture model. All of the above cocultured cells were incubated in the mixture medium that corresponded to the cocultured cells in terms of categories and ratios.

2.5. Cell proliferation and attachment assay

Cell proliferation was analyzed using a cell counting kit-8 (CCK-8, Beyotime, China) assay. Monocultured and cocultured cells

were seeded on scaffolds for 1, 3, and 7 days. The absorbance was measured at a wavelength of 450 nm in a microplate reader (Epoch microplate spectrophotometer, BioTek, USA). Cell morphology and adhesion were observed after 1 and 7 days in the four-cell coculture model. Cell-seeded scaffolds were rinsed once with phosphate-buffered saline (PBS, Sangon Biotech, China) and fixed with 2.5% glutaraldehyde, followed by dehydration in graded ethanol (30%, 40%, 50%, 60%, 70%, 80%, 90%, 95%, and 100% (v/v)).

2.6. Separation of HBMSCs and HUVECs using magnetic beads

To measure the gene expression of each kind of cell motivated by another in the two-cell coculture models, magnetic beads were used to separate the cocultured cells. In the HBMSC–HUVEC coculture model, all cells were trypsinized and centrifuged. The cells were then resuspended in the buffer solution, PBS with 0.1% bovine serum albumin (BSA, Sangon Biotech, China) with Dynabeads (Invitrogen, USA) combined with the cluster of differentiation (CD) 31 antibody. After being incubated for 20 min at 4 °C, the cell suspension was placed in a magnet for 2 min and the supernatant was transferred to a new tube. This separation process was repeated three times to obtain high-purity isolated cells. The separated HBMSCs and HUVECs in the coculture system are referred to herein as Co-HBMSCs and Co-HUVECs, respectively.

2.7. Quantitative real-time polymerase chain reaction

To evaluate the messenger RNA (mRNA) expression levels of osteogenic-specific genes (*BMP2*, *Runx2*, *ALP*, *OCN*, and *Col1*) and angiogenic-specific genes (*VEGF*, *KDR*, *eNOS*, and *VE-Cad*) in the monocultured cells and in the separated and non-separated cocultured cells, the total RNA was extracted using TRIzol reagent (Invitrogen, USA) at 3 days. RNA concentrations were detected with a NanoDrop instrument (NanoDrop Technologies, Thermo, USA). Complementary DNA (cDNA) was prepared using the PrimeScript RT Master Mix kit (TaKaRa, Japan) according to the manufacturer's instructions. Real-time PCR was performed using a SYBR Green qPCR Master Mix (TaKaRa, Japan). The relative gene expression level was calculated using the cycling threshold (Ct) value comparison ($2^{-\Delta\Delta Ct}$) method. *GAPDH* was used as the housekeeping gene. The primer sequences are listed in Table 1.

2.8. Statistical analysis

All experimental data were statistically analyzed using the Student's *t*-test analysis software. The results were presented as means ± standard deviations (SDs). Differences between groups were detected by *t*-test, and $p < 0.05$ was considered to be a significant difference between groups.

3. Results

3.1. Characterization of 3D-printed cell-container-like scaffolds

Fig. 1(a) shows that 3D-printed cell containers with different microstructures can be prepared using 3D printing technology. Figs. 1(b) and (c) provide a schematic diagram of an integrated

Table 1
Primers used for qRT-PCR.

Target gene	Forward primer sequence (5′–3′)	Reverse primer sequence (5′–3′)
GAPDH	ACGGATTTGGTCGTATTGGGCG	CTCCTGGAAGATGGTGATGG
BMP2	TTCGGCCTGAAACAGAGACC	CCTGAGTGCCTGCGATACAG
Runx2	TGGTTACTGTCATGGCGGGTA	TCTCAGATCGTTGAACCTTGCTA
ALP	ACCACCACGAGAGTGAACCA	CGTTGTCTGAGTACCAGTCCC
OCN	TCACACTCCTCGCCCTATTGG	TACCTCGCTGCCCTCCTGCTT
Col1	GAGGGCCAAGACGAAGACATC	CAGATCACGTCATCGCACAAC
VEGF	TATGCGGATCAAACCTCACCA	CACAGGGATTTTTCTTGTCTTGCT
KDR	CCCAGGCTCAGCATACAAAAAGAC	CCAGTACAAGTCCCTCTGTCCC
eNOS	TGTCCAACATGCTGCTGGAAATTG	AGGAGGTCTTCTTCCTGGTGATGCC
VE-Cad	GGCTCAGACATCCACATAACC	CTTACCAGGGCGTTCAGGGAC

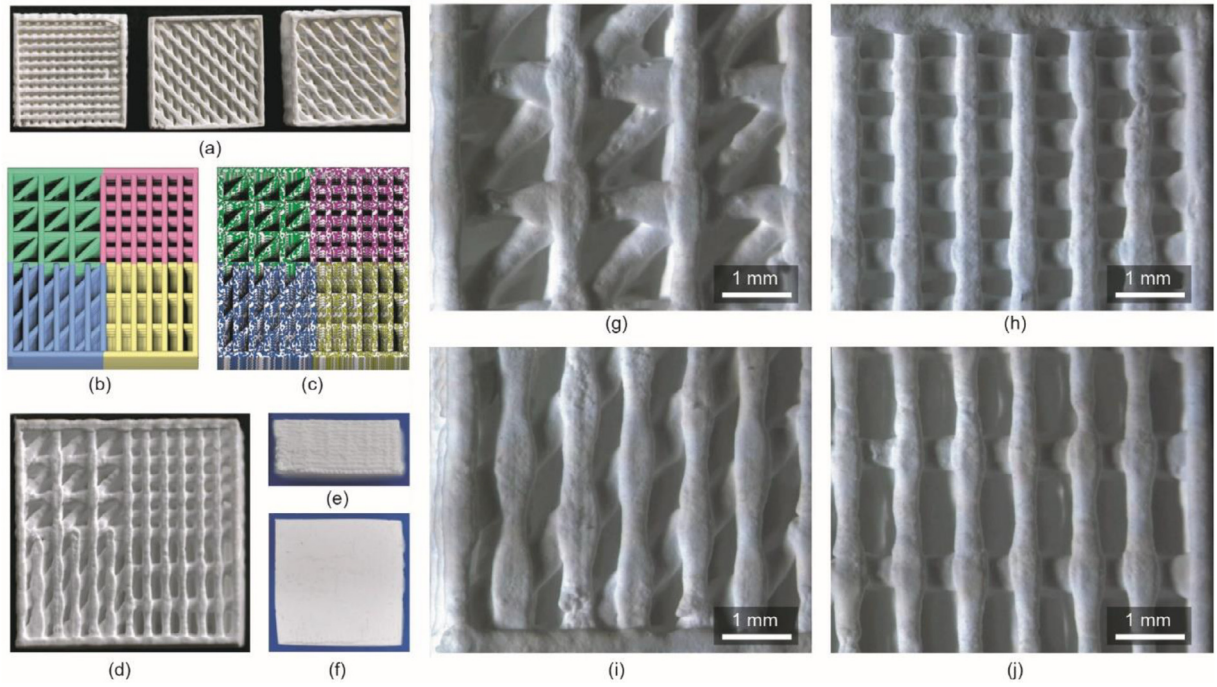

Fig. 1. Morphology of the 3D-printed cell containers. (a) Digital photograph of 3D-printed β-TCP/HA cell containers with different microstructures; schematic diagram of the 3D cell containers (b) with or (c) without different cell lines; (d) front view, (e) side view, and (f) rear view of a 3D cell container; micrographs of 3D cell containers with four combinations of pore structures including (g) triangles, (h) squares, (i) parallelograms, and (j) rectangles. Note that (g)–(j) are higher magnification images from (d).

3D cell container that combines four different pore structures (triangle, square, parallelogram, and rectangle) with or without seeded cells. A non-contact coculture model with four kinds of cells was established by seeding different cells into the four parts of the scaffolds. Using an extrusion-based 3D printer, microstructured scaffolds were fabricated with a well-defined geometry (Figs. 1(d) and (g)–(j)). From the scanning electron microscopy (SEM) micrographs, it is clear that all the walls, bottom, and boundaries of the different microstructured parts are seamlessly connected, such that a sealed cell container was manufactured (Figs. 1(d)–(f)). The XRD composition analysis of the printed cell container is shown in Fig. 2, indicating that β-TCP/HA biphasic scaffolds were obtained after sintering.

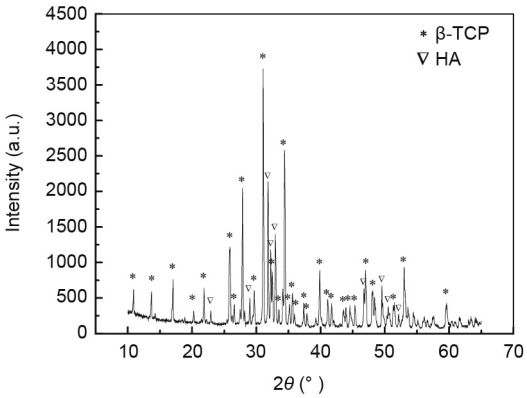

Fig. 2. XRD analysis of the 3D-printed β-TCP/HA biphasic bioceramic scaffolds. a.u.: arbitrary units; 2θ: scattering angle.

3.2. Cell viability and morphology in monoculture and coculture models

The SEM images in Fig. 3 show the cell morphology of the cocultured HBMSCs, HUVECs, HUVSMCs, and HDFs on the prescribed parts of the scaffolds at days 1 and 7. All the cocultured cells spread well, showing affluent pseudopods at day 1 and covering the whole scaffold at day 7. Fig. 4 shows the cell proliferation of the monocultured and cocultured cells in the scaffolds at different times. The results indicate that the non-contact coculture cell models in the 3D printing scaffolds showed a significant advantage in enhanced cell viability. Higher proliferation rate was observed in the cocultured HBMSC/HUVEC/HUVSMC group and in the cocultured HBMSC/HUVEC/HUVSMC/HDF group in comparison with the monocultured groups at days 3 and 7. The cocultured HBMSC/HUVEC/HUVSMC/HDF group exhibited the highest proliferation efficiency.

3.3. Osteogenic and angiogenic effects and cell–cell interactions of HBMSCs and HUVECs in 3D coculture models

To investigate the effects of the non-contact 3D coculture model on the cell–cell interactions, an *in vitro* coculture system with HBMSCs and HUVECs in 3D cell containers was applied. After coculturing for 3 days, the two types of cells were separated from the cell containers and the expression of osteogenic genes (*BMP2*, *Runx2*, *ALP*, *OCN*, and *Col1*) and angiogenic genes (*VEGF*, *KDR*, *eNOS*, and *VE-Cad*) from the separated cells were measured (Figs. 5 and 6). In general, the expression of osteogenic and angiogenic genes was found to be significantly upregulated in the non-contact 3D culture system in both the monocultured cells and the separated

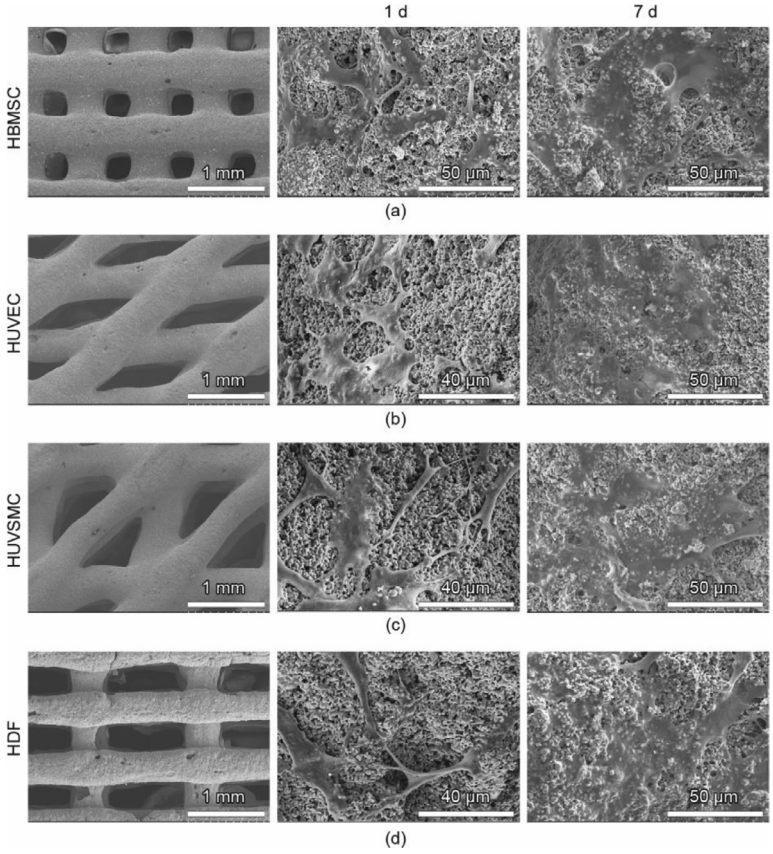

Fig. 3. SEM analysis of the cell morphology of (a) HBMSCs in the square pores, (b) HUVECs in the parallelogram pores, (c) HUVSMCs in the triangular pores, and (d) HDFs in the rectangular pores on 3D-printed β-TCP/HA cell containers, respectively, after culturing for 1 and 7 d.

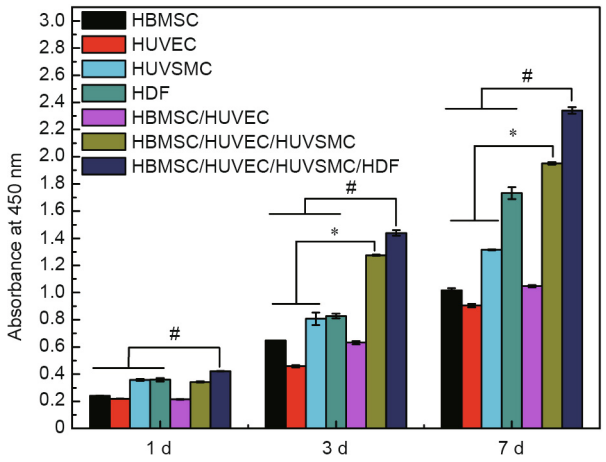

Fig. 4. CCK-8 analysis of the cell proliferation of monocultured cells and cocultured cells in 3D-printed β-TCP/HA cell containers at days 1, 3, and 7, respectively. HBMSC, HUVEC, HUVSMC, and HDF: monocultured HBMSCs, HUVECs, HUVSMCs, or HDFs in 3D cell containers; HBMSC/HUVEC: HBMSCs first seeded in the square and rectangular pores of the 3D cell containers, and then cocultured with HUVECs in the parallelogram and triangular pores; HBMSC/HUVEC/HUVSMC: HBMSCs first seeded in the square and rectangular pores of the 3D cell containers, and then cocultured with HUVECs in the parallelogram pores and HUVSMCs in the triangular pores; HBMSC/HUVEC/HUVSMC/HDF: HBMSCs first seeded in the square pores of the 3D cell containers, and then cocultured with HUVECs in the parallelogram pores, HUVSMCs in the triangular pores, and HDFs in the rectangular pores. * represents significant difference ($p < 0.05$) for the cocultured HBMSC/HUVEC/HUVSMC groups compared with the monocultured HBMSC, HUVEC, and HUVSMC groups, respectively; # represents significant difference ($p < 0.05$) for the cocultured HBMSC/HUVEC/HUVSMC/HDF groups compared with the monocultured HBMSC, HUVEC, HUVSMC, and HDF groups, respectively ($n = 6$ for each group).

cocultured cells, in comparison with the 2D culture system. More interestingly, in the HBMSC/HUVEC coculture system, *BMP2*, the bone-related gene, was mainly expressed by the Co-HUVECs, and the *BMP2* expressed by the Co-HUVECs in the 3D coculture model was significantly higher than that expressed by the Co-HUVECs in the 2D coculture model. In addition, vascular endothelial growth factor (*VEGF*), which promotes angiogenesis, was mainly expressed by the Co-HBMSCs, and the expression of *VEGF* in the Co-HBMSCs in the 3D coculture model was significantly higher than that in the 2D coculture model. Furthermore, the Co-HBMSCs in the 3D scaffolds showed significantly improved levels of *Runx2*, *ALP*, *OCN*, and *Col1*, while *KDR*, *eNOS*, and *VE-Cad* were mainly expressed by the Co-HUVECs in the 3D scaffolds.

3.4. Osteogenic and angiogenic effects of multicell cocultures in 3D coculture models

The osteogenic and angiogenic marker gene expression of monocultured (HBMSC, HUVEC) and cocultured (HBMSC/HUVEC, HBMSC/HUVEC/HUVSMC, and HBMSC/HUVEC/HUVSMC/HDF) cells in the 3D cell containers was distinctly higher than that in the 2D cell culture plate (Figs. 7 and 8). In the 3D multicell coculture system, the coculture modes (including two-cell cocultures, three-cell cocultures, and four-cell cocultures) all showed obvious advantages in enhancing osteogenic and angiogenic differentiation, in comparison with the monoculture modes. Expression of the osteogenic genes *Runx2*, *ALP*, *OCN*, and *Col1*, and of the angiogenic genes *VEGF*, *KDR*, *eNOS*, and *VE-Cad*, was significantly improved with the addition of HUVSMCs and HDFs in the coculture system, and the four-cell non-contact coculture mode (HBMSC/HUVEC/HUVSMC/HDF) in the 3D cell container exhibited optimal osteogenic and angiogenic activities.

4. Discussion

One possible reason for failure in the construction of the complex structures and functions of tissues and organs is that there are no suitable engineered cell culture models that can mimic the multicellular components of human tissues. The establishment of tissue-specific multicellular coculture systems at a 3D level is critical for the investigation of cell–cell interactions and for further preparation of engineered tissues *in vitro*. In the past few years, 3D coculture systems have been widely designed and used in

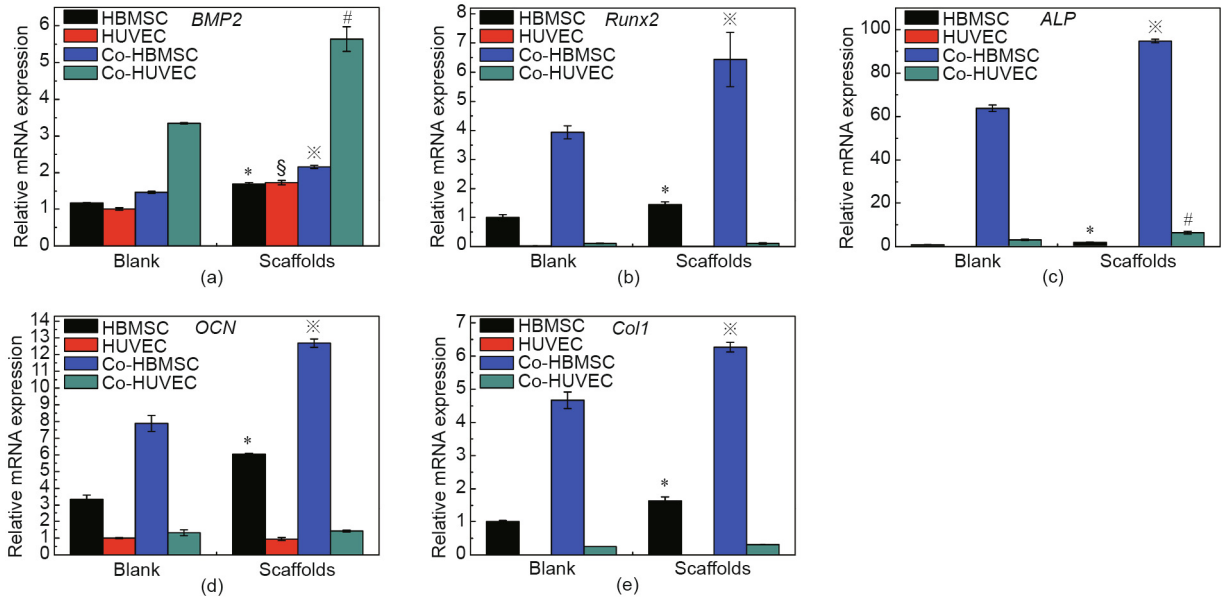

Fig. 5. Expression of the osteogenic marker genes (a) *BMP2*, (b) *Runx2*, (c) *ALP*, (d) *OCN*, and (e) *Col1* by cells cultured in cell culture plates and 3D cell containers. "Blank" refers to cells cultured in cell culture plates and "Scaffolds" refers to cells cultured in 3D cell containers. HBMSC, HUVEC: monocultured HBMSCs or HUVECs; Co-HBMSC: separated HBMSCs from the cocultured HBMSCs/HUVECs; Co-HUVEC: separated HUVECs from the cocultured HBMSCs/HUVECs. *, §, ※, and # indicate significant differences ($p < 0.05$) in the gene expression of HBMSC, HUVEC, Co-HBMSC, and Co-HUVEC, respectively, between the β-TCP/HA scaffolds and the "Blank" groups ($n = 3$ for each group).

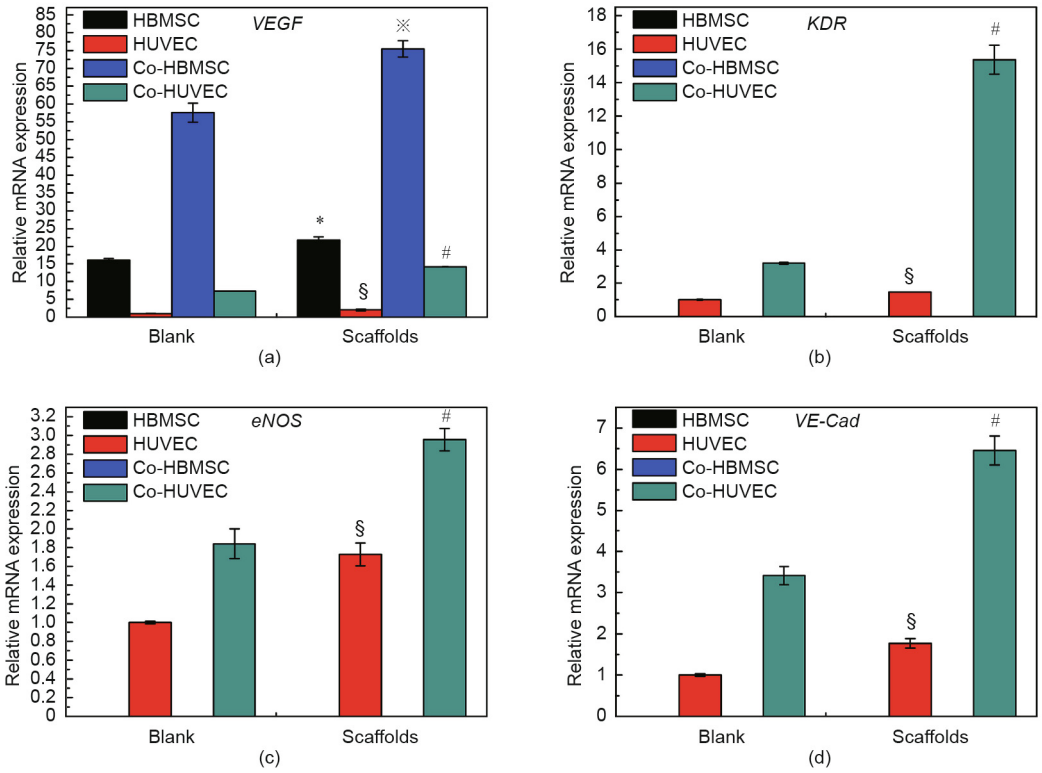

Fig. 6. Expression of the angiogenic marker genes (a) *VEGF*, (b) *KDR*, (c) *eNOS*, and (d) *VE-Cad* by cells cultured in cell culture plates and 3D cell containers. "Blank" refers to cells cultured in cell culture plates and "Scaffolds" refers to cells cultured in 3D cell containers. HBMSC, HUVEC: monocultured HBMSCs or HUVECs; Co-HBMSC: separated HBMSCs from the cocultured HBMSCs/HUVECs; Co-HUVEC: separated HUVECs from the cocultured HBMSCs/HUVECs. *, §, ※, and # indicate significant differences ($p < 0.05$) in the gene expression of HBMSC, HUVEC, Co-HBMSC, and Co-HUVEC, respectively, between the β-TCP/HA scaffolds and the "Blank" groups ($n = 3$ for each group).

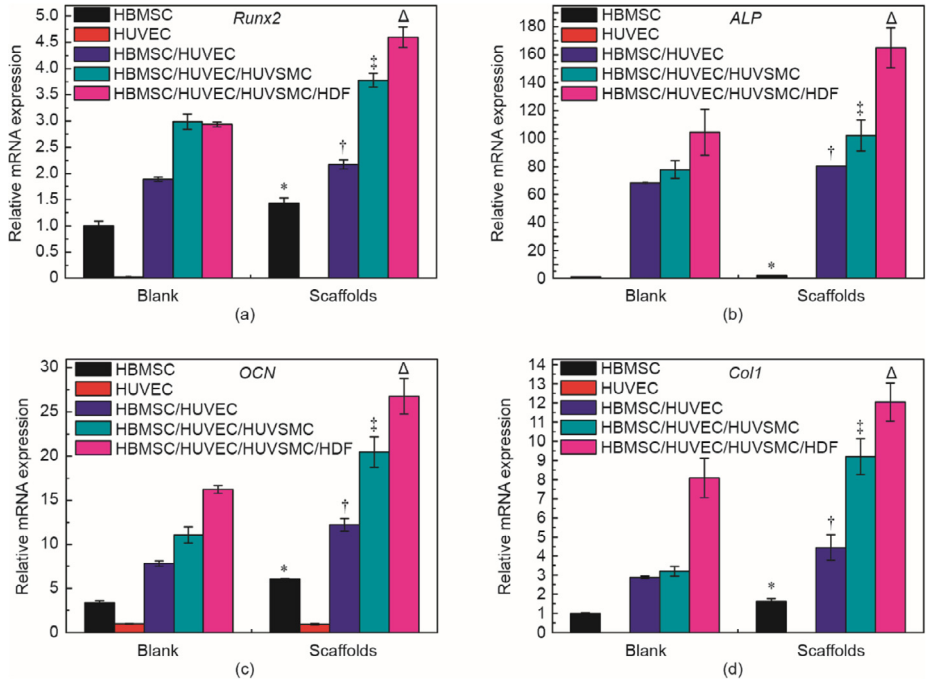

Fig. 7. Osteogenic gene expression of (a) *Runx2*, (b) *ALP*, (c) *OCN*, and (d) *Col1* by cells cultured in cell culture plates and 3D cell containers in a monoculture system or multicell coculture system. "Blank" refers to cells cultured in cell culture plates and "Scaffolds" refers to cells cultured in 3D cell containers. HBMSC, HUVEC: monocultured HBMSCs or HUVECs; HBMSC/HUVEC: HBMSC and HUVEC two-cell coculture system; HBMSC/HUVEC/HUVSMC: HBMSC, HUVEC, and HUVSMC three-cell coculture system; HBMSC/HUVEC/HUVSMC/HDF: HBMSC, HUVEC, HUVSMC, and HDF four-cell coculture system. *, †, ‡, and Δ indicate significant differences ($p < 0.05$) in the gene expression of HBMSC, HBMSC/HUVEC, HBMSC/HUVEC/HUVSMC, and HBMSC/HUVEC/HUVSMC/HDF, respectively, between the β-TCP/HA scaffolds and the "Blank" groups ($n = 3$ for each group).

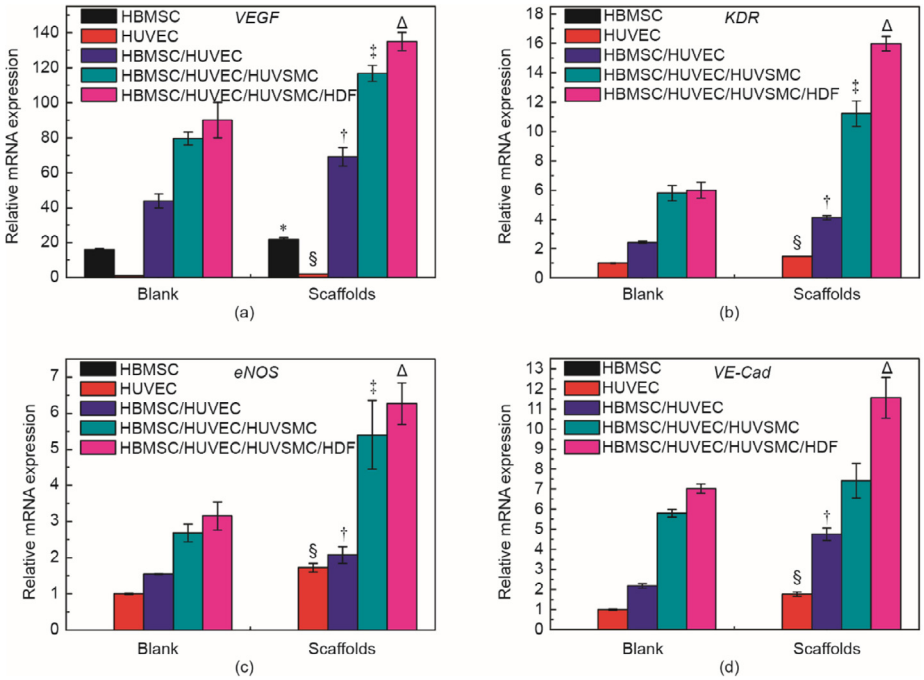

Fig. 8. Angiogenic gene expression of (a) *VEGF*, (b) *KDR*, (c) *eNOS*, and (d) *VE-Cad* by cells cultured in cell culture plates and 3D cell containers in a monoculture system or coculture system. "Blank" refers to cells cultured in cell culture plates and "Scaffolds" refers to cells cultured in 3D cell containers. HBMSC, HUVEC: monocultured HBMSCs or HUVECs; HBMSC/HUVEC: HBMSC and HUVEC two-cell coculture system; HBMSC/HUVEC/HUVSMC: HBMSC, HUVEC, and HUVSMC three-cell coculture system; HBMSC/HUVEC/HUVSMC/HDF: HBMSC, HUVEC, HUVSMC, and HDF four-cell coculture system. *, §, †, ‡, and Δ indicate significant differences ($p < 0.05$) in the gene expression of HBMSC, HUVEC, HBMSC/HUVEC, HBMSC/HUVEC/HUVSMC, and HBMSC/HUVEC/HUVSMC/HDF, respectively, between the β-TCP/HA scaffolds and the "Blank" groups ($n = 3$ for each group).

mimicking the physiological environment *in vivo*, and a handful of works have focused on seeding a mixed suspension of cocultured cells into a homogenous porous scaffold or a collagen, fibrin, or silk gel [21–25]. Although previous studies have demonstrated that simply mixing multiple cells together in 3D niches was effective in enhancing cell proliferation and differentiation compared with traditional 2D coculture [26], most cells communicate with each other in a non-contact manner *in vivo*. Therefore, developing a 3D non-contact multicell coculture container for sufficient cell–cell communication is a new strategy for tissue engineering.

Although numerous methods, such as molding and ice templating, have been developed to fabricate cell-containing scaffolds, the prepared pore structure is not optimal. It is well known that 3D printing is a preferred technology to efficiently prepare complex-structure scaffolds with a variety of pore sizes and morphologies [27–31]. In this study, we successfully fabricated a β-TCP/HA composite scaffold with four different pore structures including triangles, squares, parallelograms, and rectangles by using an extrusion-based 3D printing method (Fig. 1). Previous studies have found that a large number of cells leaked out of the 3D-printed porous scaffold during the cell-seeding operations. The present study fabricated a cell container in which the walls, bottom, and boundaries among the different microstructured parts of the scaffold were seamlessly connected. This method allowed precise control of the cell-seeding density and ratio to be achieved, without cell suspension loss. It has been reported that the porous structure and pore morphology of the scaffold are important in influencing the cell response, including cell attachment and proliferation, nutrient transport, and tissue growth [32–35]. The present study found that the 3D non-contact cell containers with different pore structures not only promoted the proliferation of a single type of cell, but also significantly stimulated the proliferation of cocultured cells. In particular, the coculture of three or four kinds of cells with a 3D scaffold exhibited a significant advantage in stimulating cell proliferation compared with a single cell type, indicating that cell–cell interactions and communications had taken place in the 3D non-contact cell container. There may be multiple potential molecular mechanisms in the scaffold-regulated cell proliferation; we tend to believe that the 3D cell-container-like scaffold might, on the one hand, affect the cytoskeleton through structural effects, which activate cell-proliferation-related signaling pathways and promote cell proliferation and, on the other hand, enhance cell proliferation by amplifying the paracrine effect of the cocultured cells. Of course, these hypotheses require further confirmation.

To clarify the roles of the 3D cell containers in affecting cell-to-cell communications, we first selected a relatively simple two-cell coculture system with HBMSCs and HUVECs. A previous study on a 2D direct-contact HBMSC/HUVEC coculture system demonstrated that the angiogenic growth factor VEGF secreted from the HBMSCs promoted the activation of *KDR* in the HUVECs, which further enhanced the expression of *BMP2* and *eNOS* to initiate osteogenesis and angiogenesis [12]. Our study demonstrates that the synergistic effect of HBMSCs and HUVECs in osteogenesis and angiogenesis is amplified in a scaffold-based 3D indirect coculture system, as characterized by the remarkable upregulation of the expression of osteogenic and angiogenic genes by the separated cocultured cells in the 3D model compared with the 2D model. Interestingly, our experiments revealed that the angiogenic growth factor VEGF was mainly expressed by the Co-HBMSCs, and that the expression of *VEGF* by the Co-HBMSCs in the 3D coculture model was significantly higher than that in the 2D coculture model. Simultaneously, the expression of *VEGF* receptors such as *KDR* from the cocultured HUVECs in the 3D cell containers was significantly enhanced. In addition, the Co-HUVECs in the 3D scaffolds showed higher upregulation of angiogenic genes such as *eNOS* and *VE-Cad*. It has been reported that HBMSCs might promote angiogenesis via the microstructure-sensitive paracrine effect in a coculture of HBMSCs and HUVECs in 3D substrates compared with 2D substrates [36]. It is therefore reasonable to speculate that, in comparison with a 2D

cell culture plate, a cell container with a 3D porous structure would enhance the angiogenic effect of the cocultures, probably because it would amplify the paracrine effect of the coculture system. In addition to VEGF, another important growth factor, BMP2, has been found to play an important role in the early stages of bone regeneration [37,38]. Interestingly, our results found that BMP2 was mainly expressed by the Co-HUVECs, and that the BMP2 expressed by the Co-HUVECs in the 3D coculture model was significantly higher than that expressed in the 2D coculture model. It has been reported that the BMP2 secreted by the HUVECs can regulate the osteogenesis of the HBMSCs [12]. Our results also demonstrated that the Co-HBMSCs in the 3D scaffold showed higher upregulation of osteogenic genes such as *Runx2*, *ALP*, *OCN*, and *Col1*. Based on these findings, it is clear that in the HBMSC/HUVEC coculture system at the 3D level, the VEGF expressed by the Co-HBMSCs can act on the Co-HUVECs: On the one hand, it activates their surface *VEGF* receptor *KDR*, which promotes the expression of downstream genes such as *eNOS* and *VE-Cad* in the Co-HUVECs to initiate angiogenesis; on the other hand, it stimulates the expression of *BMP2* in the Co-HUVECs, which promotes the expression of downstream genes such as *Runx2*, *ALP*, *OCN*, and *Col1* in the Co-HBMSCs to initiate osteogenesis. Our results suggest that the prepared cell container provided a good 3D environment for cell–cell interactions and communications via a paracrine pathway.

In the past decades, growth factors for enhanced angiogenesis and osteogenesis have been widely used in bone tissue engineering applications, and many studies have reported that the addition of growth factors BMP2 and VEGF into tissue engineering scaffolds can enhance the osteogenic and angiogenic activities of biomaterials [39–41]. However, the application of exogenous growth factors is limited in clinical use, due to the challenges of activity maintenance and controlled delivery [42,43]. In the present study, the 3D cell containers activated the two major biological events of osteogenesis and angiogenesis during bone tissue regeneration by increasing the expression of *BMP2* and *VEGF* from the cocultured cells. This result indicates that the engineered 3D coculture model created an environment in which cells could communicate with each other and further secrete endogenous growth factors for enhanced tissue regeneration. Our results provide a new strategy for tissue engineering construction.

As bone formation is a vascular-dependent process, angiogenesis plays a key role in bone repair and skeletal development [44,45]. In addition to endothelial cells, smooth muscle cells and fibroblasts are the major cellular components of the blood vessel wall, and these cells interact with each other in a more complex autocrine and paracrine manner to maintain the homeostasis of the blood vessels [46–48]. In this study, we added smooth muscle cells and fibroblasts into the HBMSC/HUVEC two-cell coculture system and constructed three-cell and four-cell coculture systems to study the effects of multicellular coculture modes at the 3D level on the osteogenesis and angiogenesis of the cocultures. Our results show that the three-cell cocultures and four-cell cocultures both showed obvious advantages in enhancing osteogenic and angiogenic differentiation, in comparison with the monoculture and two-cell coculture modes. Expression of the osteogenic genes *Runx2*, *ALP*, *OCN*, and *Col1* and the angiogenic genes *VEGF*, *KDR*, *eNOS*, and *VE-Cad* improved significantly with the addition of HUVSMCs and HDFs to the coculture system. Furthermore, the four-cell non-contact coculture mode (HBMSC/HUVEC/HUVSMC/HDF) in the 3D cell container exhibited optimal osteogenic and angiogenic activities. Our results demonstrate that the development of a 3D scaffold-based multicellular non-contact coculture system permits the construction of a variety of cell cocultures of physiological tissues, which is very helpful for mimicking the tissue microenvironment *in vivo* and for further tissue regeneration.

5. Conclusions

In this study, we successfully fabricated a cell-container-like β-TCP/HA scaffold with four different pore structures including triangles, squares, parallelograms, and rectangles by means of 3D printing technology. Using this scaffold, an engineered 3D coculture model composed of HBMSCs, HUVECs, HUVSMCs, and HDFs with spatially controlled distribution was constructed to mimic the cell microenvironment of human bone tissue. The 3D-printed cell-container-like scaffolds demonstrated obvious advantages in enhancing cell proliferation as well as osteogenic and angiogenic differentiation in the coculture modes, in comparison with 2D planar cultures. In the two-cell coculture mode, the interactions between HBMSCs and HUVECs suggested that the 3D cell containers with different porous structures enhanced the angiogenic and osteogenic effects of the cocultures by amplifying the paracrine effect of the coculture system, in which the stimulation of the expression of *VEGF* and *BMP2* plays a key role. Moreover, the four-cell non-contact coculture modes (HBMSC/HUVEC/HUVSMC/HDF) in the 3D cell containers exhibited optimal osteogenic and angiogenic activities. Our study indicates a new direction for developing a scaffold-based multicellular non-contact coculture system toward tissue regeneration.

Acknowledgements

The research was supported by the National Key Research and Development Program of China (2016YFB0700803), the National Natural Science Foundation of China (51761135103), Cross-disciplinary Collaborative Teams Program for Science, Technology and Innovation of Chinese Academy of Sciences (JCTD-2018-13), STS Science and Technology Service Network Plan of Chinese Academy of Science (KFJ-STS-QYZD-092), Science and Technology Commission of Shanghai Municipality (17441903700), and the German Research Foundation (DFG, GE1133/24-1).

Compliance with ethics guidelines

Xiaoya Wang, Meng Zhang, Jingge Ma, Mengchi Xu, Jiang Chang, Michael Gelinsky, and Chengtie Wu declare that they have no conflict of interest or financial conflicts to disclose.

References

[1] Langer R, Vacanti J. Tissue engineering. Science 1993;260(5110):920–6.
[2] Hopkins AM, DeSimone E, Chwalek K, Kaplan DL. 3D *in vitro* modeling of the central nervous system. Prog Neurobiol 2015;125:1–25.
[3] Giger RJ, Hollis ER, Tuszynski MH. Guidance molecules in axon regeneration. Cold Spring Harbor Perspect Biol 2010;2(7):a001867.
[4] Annabi N, Tamayol A, Uquillas JA, Akbari M, Bertassoni LE, Cha C. 25th Anniversary Article: rational design and applications of hydrogels in regenerative medicine. Adv Mater 2014;26(1):85–124.
[5] Akbari M, Tamayol A, Bagherifard S, Serex L, Mostafalu P, Faramarzi N. Textile technologies and tissue engineering: a path toward organ weaving. Adv Healthc Mater 2016;5(7):751–66.
[6] Gu Q, Hao J, Lu Y, Wang L, Wallace GG, Zhou Q. Three-dimensional bio-printing. Sci China Life Sci 2015;58(5):411–9.
[7] Antoni D, Burckel H, Josset E, Noel G. Three-dimensional cell culture: a breakthrough *in vivo*. Int J Mol Sci 2015;16(3):5517–27.
[8] Park SB, Lee SY, Jung WH, Lee J, Jeong HG, Hong J. Development of *in vitro* three-dimensional co-culture system for metabolic syndrome therapeutic agents. Diabetes Obes Metab 2019;21(5):1146–57.
[9] Knight E, Przyborski S. Advances in 3D cell culture technologies enabling tissue-like structures to be created *in vitro*. J Anat 2015;227(6):746–56.
[10] Battiston KG, Cheung JWC, Jain D, Santerre JP. Biomaterials in co-culture systems: towards optimizing tissue integration and cell signaling within scaffolds. Biomaterials 2014;35(15):4465–76.
[11] Li H, Chang J. Bioactive silicate materials stimulate angiogenesis in fibroblast and endothelial cell co-culture system through paracrine effect. Acta Biomater 2013;9(6):6981–91.
[12] Li H, Xue Ke, Kong Ni, Liu K, Chang J. Silicate bioceramics enhanced vascularization and osteogenesis through stimulating interactions between

endothelia cells and bone marrow stromal cells. Biomaterials 2014;35(12):3803–18.
[13] Clarke MSF, Sundaresan A, Vanderburg CR, Banigan MG, Pellis NR. A three-dimensional tissue culture model of bone formation utilizing rotational co-culture of human adult osteoblasts and osteoclasts. Acta Biomater 2013;9(8):7908–16.
[14] Kang Y, Kim S, Fahrenholtz M, Khademhosseini A, Yang Y. Osteogenic and angiogenic potentials of monocultured and co-cultured human-bone-marrow-derived mesenchymal stem cells and human-umbilical-vein endothelial cells on three-dimensional porous beta-tricalcium phosphate scaffold. Acta Biomater 2013;9(1):4906–15.
[15] Kook YM, Jeong Y, Lee K, Koh WG. Design of biomimetic cellular scaffolds for co-culture system and their application. J Tissue Eng 2017;8. 204173141772464.
[16] Levorson EJ, Santoro M, Kurtis Kasper F, Mikos AG. Direct and indirect co-culture of chondrocytes and mesenchymal stem cells for the generation of polymer/extracellular matrix hybrid constructs. Acta Biomater 2014;10(5):1824–35.
[17] Gao B, Konno T, Ishihara K. Quantitating distance-dependent, indirect cell–cell interactions with a multilayered phospholipid polymer hydrogel. Biomaterials 2014;35(7):2181–7.
[18] Feng C, Zhang W, Deng C, Li G, Chang J, Zhang Z, Jiang X, Wu C. 3D printing of lotus root-like biomimetic materials for cell delivery and tissue regeneration. Adv Sci 2017;4(12):1700401.
[19] Li H, Daculsi R, Grellier M, Bareille R, Bourget C, Amedee J. Role of neural-cadherin in early osteoblastic differentiation of human bone marrow stromal cells cocultured with human umbilical vein endothelial cells. Am J Physiol-Cell Physiol 2010;299(2):C422–30.
[20] Sorrell JM, Baber MA, Brinon L, Carrino DA, Seavolt M, Asselineau D, et al. Production of a monoclonal antibody, DF-5, that identifies cells at the epithelial-mesenchymal interface in normal human skin. APN/CD13 is an epithelial-mesenchymal marker in skin. Exp Dermatol 2003;12(3):315–23.
[21] Lai N, Jayaraman A, Lee K. Enhanced proliferation of human umbilical vein endothelial cells and differentiation of 3T3-L1 adipocytes in coculture. Tissue Eng Part A 2009;15(5):1053–61.
[22] Saiki A, Watanabe F, Murano T, Miyashita Y, Shirai K. Hepatocyte growth factor secreted by cultured adipocytes promotes tube formation of vascular endothelial cells *in vitro*. Int J Obes 2006;30(11):1676–84.
[23] Kang JH, Gimble JM, Kaplan DL. *In vitro* 3D model for human vascularized adipose tissue. Tissue Eng Part A 2009;15(8):2227–36.
[24] Borges J, Müller MC, Momeni A, Björn Stark G, Torio-Padron N. *In vitro* analysis of the interactions between preadipocytes and endothelial cells in a 3D fibrin matrix. Minim Invasiv Ther 2007;16(3):141–8.
[25] Choi JH, Bellas E, Gimble JM, Vunjak-Novakovic G, Kaplan DL. Lipolytic function of adipocyte/endothelial cocultures. Tissue Eng Part A 2011;17(9–10):1437–44.
[26] Zhu W, Castro NJ, Cui H, Zhou X, Boualam B, McGrane R, et al. A 3D printed nano bone matrix for characterization of breast cancer cell and osteoblast interactions. Nanotechnology 2016;27(31):315103.
[27] Rao RB, Krafcik KL, Morales AM, Lewis JA. Microfabricated deposition nozzles for direct-write assembly of three-dimensional periodic structures. Adv Mater 2005;17(3):289–93.
[28] Therriault D, Shepherd RF, White SR, Lewis JA. Fugitive inks for direct-write assembly of three-dimensional microvascular networks. Adv Mater 2005;17(4):395–9.
[29] Lee SH, Jeong HE, Park MC, Hur JY, Cho HS, Park SH. Fabrication of hollow polymeric microstructures for shear-protecting cell-containers. Adv Mater 2008;20(4):788–92.
[30] Truckenmüller R, Giselbrecht S, Escalante-Marun M, Groenendijk M, Papenburg B, Rivron N. Fabrication of cell container arrays with overlaid surface topographies. Biomed Microdevices 2012;14(1):95–107.
[31] Oh HH, Ko YG, Lu H, Kawazoe N, Chen G. Preparation of porous collagen scaffolds with micropatterned structures. Adv Mater 2012;24(31):4311–6.
[32] Hutmacher DW. Scaffolds in tissue engineering bone and cartilage. Biomaterials 2000;21(24):2529–43.
[33] Yun HS, Park JW, Kim SH, Kim YJ, Jang JH. Effect of the pore structure of bioactive glass balls on biocompatibility *in vitro* and *in vivo*. Acta Biomater 2011;7(6):2651–60.
[34] Cho SY, Park HH, Jin HJ. Controlling pore size of electrospun silk fibroin scaffold for tissue engineering. Polym-Korea 2012;36(5):651–5.
[35] Xu M, Zhai D, Chang J, Wu C. *In vitro* assessment of three-dimensionally plotted nagelschmidtite bioceramic scaffolds with varied macropore morphologies. Acta Biomater 2014;10(1):463–76.
[36] Martín-Saavedra F, Crespo L, Escudero-Duch C, Saldaña L, Gómez-Barrena E, Vilaboa N. Substrate microarchitecture shapes the paracrine crosstalk of stem cells with endothelial cells and osteoblasts. Sci Rep 2017;7(1):15182.
[37] Yu YY, Lieu S, Lu C, Colnot C. Bone morphogenetic protein 2 stimulates endochondral ossification by regulating periosteal cell fate during bone repair. Bone 2010;47(1):65–73.
[38] Zhai D, Xu M, Liu L, Chang J, Wu C. Silicate-based bioceramics regulating osteoblast differentiation through a BMP2 signalling pathway. J Mater Chem B 2017;5(35):7297–306.
[39] Dou DD, Zhou G, Liu HW, Zhang J, Liu ML, Xiao XF. Sequential releasing of VEGF and BMP-2 in hydroxyapatite collagen scaffolds for bone tissue engineering: design and characterization. Int J Biol Macromol 2019;123:622–8.
[40] Subbiah R, Du P, Hwang MP, Kim IG, Van SY, Noh YK. Dual growth factor-loaded core-shell polymer microcapsules can promote osteogenesis and angiogenesis. Macromol Res 2014;22(12):1320–9.
[41] Kim M, Jung WK, Kim G. Bio-composites composed of a solid free-form fabricated polycaprolactone and alginate-releasing bone morphogenic protein and bone formation peptide for bone tissue regeneration. Bioprocess Biosyst Eng 2013;36(11):1725–34.
[42] Han Y, Li Y, Zeng Q, Li H, Peng J, Xu Y. Injectable bioactive akermanite/alginate composite hydrogels for *in situ* skin tissue engineering. J Mater Chem B 2017;5(18):3315–26.
[43] Mitchell AC, Briquez PS, Hubbell JA, Cochran JR. Engineering growth factors for regenerative medicine applications. Acta Biomater 2016;30:1–12.
[44] Matsumoto T, Goto D, Sato S. Subtraction micro-computed tomography of angiogenesis and osteogenesis during bone repair using synchrotron radiation with a novel contrast agent. Lab Invest 2013;93(9):1054–63.
[45] Kanczler JM, Oreffo ROC. Osteogenesis and angiogenesis: the potential for engineering bone. Eur Cells Mater 2008;15:100–14.
[46] Mantella LE, Quan A, Verma S. Variability in vascular smooth muscle cell stretch-induced responses in 2D culture. Vasc cell 2015;7(1):7–16.
[47] Anwar MA, Shalhoub J, Lim CS, Gohel MS, Davies AH. The effect of pressure-induced mechanical stretch on vascular wall differential gene expression. J Vasc Res 2012;49(6):463–78.
[48] Lemarié CA, Tharaux PL, Lehoux S. Extracellular matrix alterations in hypertensive vascular remodeling. J Mol Cell Cardiol 2010;48(3):433–9.